Key Points:
- A depression allows persistent access of warm (up to ~1°C) Modified Circumpolar Deep Water (MCDW) to the inner continental shelf
- Observed MCDW intrusions were warmer and thicker in austral autumn and early winter than in other seasons
- Seasonality of the flow on the continental slope explains the seasonality of the MCDW intrusions onto the inner continental shelf

Seasonality of Warm Water Intrusions Onto the Continental Shelf Near the Totten Glacier

Alessandro Silvano[1,2,3] (iD), **Stephen R. Rintoul**[2,3,5] (iD), **Kazuya Kusahara**[3,4] (iD), **Beatriz Peña-Molino**[2,3,5] (iD), **Esmee van Wijk**[2,3], **David E. Gwyther**[1] (iD), and **Guy D. Williams**[1,3,6] (iD)

[1]Institute for Marine and Antarctic Studies, University of Tasmania, Hobart, Tasmania, Australia, [2]CSIRO Oceans and Atmosphere, Hobart, Tasmania, Australia, [3]Antarctic Climate and Ecosystems Cooperative Research Centre, University of Tasmania, Hobart, Tasmania, Australia, [4]Japan Agency for Marine-Earth Science and Technology, Yokohama, Japan, [5]Centre for Southern Hemisphere Oceans Research, Hobart, Tasmania, Australia, [6]Antarctic Research Council Centre of Excellence for Climate System Science, University of New South Wales, Sydney, New South Wales, Australia

Abstract Warm Modified Circumpolar Deep Water (MCDW) from the Southern Ocean drives rapid basal melt of the Totten Ice Shelf on the Sabrina Coast (East Antarctica), affecting the mass balance of the grounded Totten Glacier. Recent observations show that MCDW intrudes onto the continental shelf through a depression at the shelf break. Here we investigate such intrusions by combining (1) new oceanographic and bathymetric observations collected for two consecutive years by profiling floats in the depression south of the shelf break, (2) oceanographic measurements collected by conductivity-temperature-depth-instrumented seals on continental slope, and (3) an ocean model. The depression provides a pathway for persistent inflow of warm (0-1°C) MCDW to the inner shelf. In austral autumn and early winter MCDW intrusions were up to 0.5°C warmer and were ~75 m thicker than in spring and summer. The seasonality of the flow on the continental slope explains the seasonality of the intrusions. The MCDW layer on the continental slope is warmer and thicker to the east of the depression than to the west. In autumn and early winter a strong, top-to-bottom westward current (Antarctic Slope Current) transports the warmer and thicker MCDW layer along the slope and is diverted poleward at the eastern entrance of the depression. A bottom-intensified eastward current (Antarctic Slope Undercurrent) develops in other months, allowing cooler and thinner intrusions to enter the depression from the west. Our study illustrates how circulation on the Antarctic slope regulates the ocean heat delivery to the continental shelf and ultimately to the ice shelves.

1. Introduction

Recent satellite observations have shown that the Antarctic Ice Sheet is losing mass at an accelerating rate (Velicogna et al., 2014), with the most rapid loss observed in the Amundsen and Bellingshausen sectors of West Antarctica (Harig & Simons, 2015; Shepherd et al., 2018). The mass loss is due to acceleration of outlet glaciers that drain the Antarctic Ice Sheet into the ocean (Rignot et al., 2008). This acceleration has been attributed to thinning or collapse of the ice shelves that form where outlet glaciers reach the ocean (Pritchard et al., 2012; Scambos et al., 2004). When ice shelves thin or collapse, the backstress they exert on the grounded glaciers reduces or vanishes. This process accelerates the flow of the outlet glaciers into the ocean, resulting in a net mass loss of the Antarctic Ice Sheet that contributes to sea level rise.

The primary forcing causing ice-shelf thinning is thought to be ocean heat flux (Christianson et al., 2016; Pritchard et al., 2012). The largest reservoir of ocean heat in the Southern Ocean is the Circumpolar Deep Water (Rintoul & Naveira Garabato, 2013), a warm (2-3°C) and salty (salinity ~ 34.7) water mass found below 2,000-m depth north of 40°S. South of 40°S, the Circumpolar Deep Water shoals due to wind-driven upwelling (Greene et al., 2017; Marshall & Speer, 2012). As it moves poleward, Circumpolar Deep Water mixes with cold Antarctic waters, losing its core properties (Orsi & Wiederwohl, 2009). It is then referred to as Modified Circumpolar Deep Water (MCDW). MCDW is observed on the Antarctic continental slope near the shelf break (i.e., upper continental slope) between 400- and 1,000-m depth (e.g., Bindoff et al., 2000; Walker et al., 2013).

MCDW found on the upper slope is able to reach the continental shelf in many regions around Antarctica. The warmest intrusions are observed in West Antarctica, where MCDW on the continental shelf of the western Antarctic Peninsula (Moffat et al., 2009), Amundsen (Jacobs et al., 2012), and Bellingshausen seas
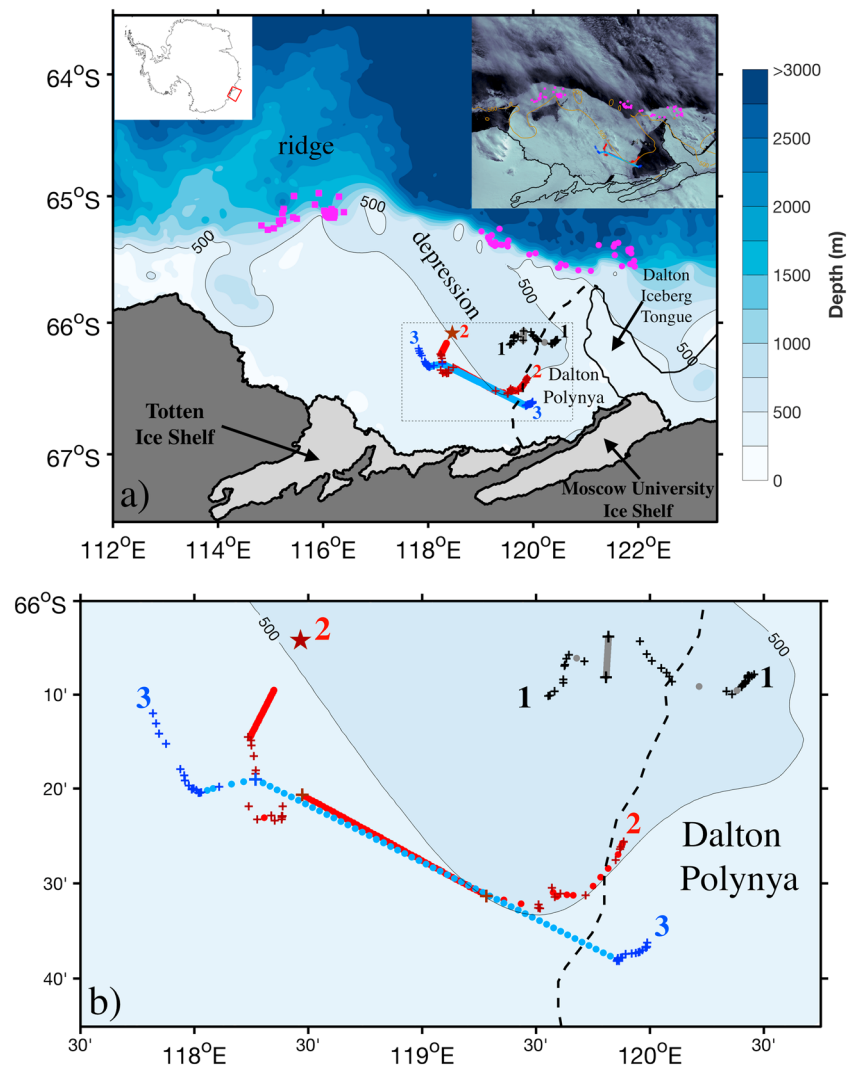
Figure 1. Sabrina Coast. (a) Map of the survey area with overlaid bathymetry and coastline (International Bathymetric Chart of the Southern Ocean [IBCSO]; Arndt et al., 2013). The upper left inset shows the model domain in Antarctica. The contour of the 500-m isobath is included in black to highlight the depression. The dashed line indicates the approximate western boundary of the Dalton Polynya, which forms in the lee of the Dalton Iceberg Tongue, the latter made from a combination of grounded icebergs and fast ice located to the north of the Moscow University Ice Shelf. The black, red, and blue symbols indicate the location of profiles collected by floats 1, 2, and 3, respectively. Lighter colored dots show interpolated locations for periods when the floats were under sea ice, while darker pluses show locations where the floats surfaced. Floats were deployed in the Dalton Polynya and then drifted to the west. The red star shows the location of the last time float 2 surfaced (November 2017). The magenta circles (squares) show the location of data collected by CTD-instrumented seals on the upper slope to the east (west) of the depression. In the upper right inset is a Moderate Resolution Imaging Spectroradiometer (MODIS, Scambos et al., 1996) image (22 January 2015) with coastline overlaid. (b) Zoom of the area delimited in (a) by the dashed black rectangle.

(Jenkins & Jacobs, 2008) is above 0.5°C. Here MCDW accesses the continental shelf in the bottom layer, overlaid by a layer of fresh and cold Winter Water that is the product of winter convection near the surface. Warm water is then able to reach the ice-shelf cavities and drive rapid basal melt at depth.

Recently, warm MCDW has been observed in the bottom layer on the continental shelf of the Sabrina Coast in East Antarctica (see Figure 1a for location; Silvano et al., 2017). Here relatively warm MCDW reaches the Totten and Moscow University ice shelves to drive rapid basal melt (Rintoul et al., 2016; Silvano et al., 2017). As in the Amundsen and Bellingshausen seas, rapid basal melt of the Totten and Moscow University ice shelves is associated with mass loss and acceleration of the grounded portion of the Totten and Moscow

University glaciers (Greenbaum et al., 2015; Li et al., 2016; Mohajerani et al., 2018; Roberts et al., 2017). These observations suggest that MCDW drives mass loss of this sector of the East Antarctic Ice Sheet (Silvano et al., 2016), which holds the equivalent of 5 m of global sea level rise (Mohajerani et al., 2018).

While the importance of MCDW for melting of ice shelves is well documented, the physical mechanisms that allow MCDW to access the Antarctic continental shelf remain poorly understood (Gille et al., 2016; Rintoul, 2018). This is mostly due to the paucity of long-term observing systems capable of collecting data over multiple seasons and years. The few existing observations suggest that the main way for warm MCDW to access the continental shelf is through glacially scoured troughs in the seafloor (e.g., Jacobs et al., 2012).

Interaction between currents on the upper continental slope and troughs at the shelf break promotes MCDW intrusions onto the continental shelf (e.g., Dinniman et al., 2018; Jenkins et al., 2016; Palóczy et al., 2018; St-Laurent et al., 2013). Easterly winds drive a westward current along most of the Antarctic slope, known as the Antarctic Slope Current (Thompson et al., 2018). The Antarctic Slope Current transports MCDW, and it is diverted poleward along isobaths when it encounters a trough, resulting in intrusions originating from the east of a trough (Klinck, 1996). Intrusions from the east of a trough are observed in the Ross Sea (Kohut et al., 2013; Orsi & Wiederwohl, 2009), Weddell Sea (Darelius et al., 2016), Bellingshausen Sea (Zhang et al., 2016), and on the Adélie Coast (Williams et al., 2008). The MCDW then follows a cyclonic circulation within the trough to reach the ice shelves (e.g., Darelius et al., 2016; Zhang et al., 2016).

Observations have revealed the presence of an eastward undercurrent (known as the Antarctic Slope Undercurrent) that forms beneath the westward Antarctic Slope Current in some locations (Chavanne et al., 2010; Heywood et al., 1998; Núñez-Riboni & Fahrbach, 2009; Walker et al., 2013). Where the undercurrent encounters a trough, its flow is diverted across the trough (Allen & Durrieu de Madron, 2009; Klinck, 1996) and a cyclonic circulation arises within the trough that steers the MCDW poleward (St-Laurent et al., 2013). In this case, MCDW intrusions originate to the west of a trough, as observed in the Amundsen Sea (Assmann et al., 2013; Walker et al., 2013).

The interaction between currents on the upper slope and troughs at the shelf break is not the only mechanism that can drive cross-shelf exchange. Other processes can also be important, including waves on the upper slope (St-Laurent et al., 2013), tidal fluctuations (Stewart et al., 2018), curvature of the isobaths (Dinniman et al., 2003), and eddy fluxes (Nøst et al., 2011; Stewart & Thompson, 2015; Thompson et al., 2014). These processes can be especially important in regions where topographic depressions are absent at the shelf break and a geostrophic flow along isobaths cannot support MCDW access to the continental shelf (Stewart et al., 2018).

In this study we focus on MCDW intrusions onto the continental shelf of the Sabrina Coast. A recent survey has revealed the presence of a deep (>500 m) depression at the shelf break that facilitates the intrusions of MCDW onto the continental shelf (Nitsche et al., 2017). Poleward of the shelf break, only the eastern edge of the depression on the inner shelf and midshelf has been sampled due to the persistent sea-ice cover to the west (Gulick et al., 2017; Fernandez et al., 2018; Silvano et al., 2017; see upper right inset in Figure 1a to visualize a typical summer sea-ice cover). MCDW up to 0.3°C was observed in the deepest (about 900 m) area surveyed (Silvano et al., 2017), confirming that warm water is transported southward through the depression. However, those data are from a summer snapshot and temporal variability of the MCDW properties intruding into the depression remains unknown, as do the processes regulating onshore transport of MCDW.

Here we show new hydrographic and bathymetric observations collected in deep areas of the depression on the inner shelf. Measurements were collected for two consecutive years by a novel application of profiling floats capable of measuring ocean properties beneath sea ice. First, the float drifted following a cyclonic circulation, as seen in other depressions around Antarctica, reaching for the first time the western flank of the depression and thus providing new bathymetric information. Second, and most relevant to our study, the floats detected the seasonal variability of the MCDW properties in the depression. Warmer MCDW was observed in autumn and early winter compared to spring and summer.

To investigate the origin of the seasonality, profiles from conductivity-temperature-depth (CTD)-instrumented seals are then used to characterize the MCDW properties on the upper continental slope. The seal observations suggest that warmer MCDW accesses the depression from the east in autumn and early winter, while

cooler MCDW enters from the west in other months. This hypothesis is finally tested with a numerical model. The model shows that a seasonal reversal of the currents transporting MCDW along the slope allows warmer intrusions in autumn and early winter and cooler intrusions during the rest of the year.

The paper has the following structure. We first describe the observational and modeling tools used (section 2, with supporting information describing the validation of the model against observations). We then report the results (section 3), starting with the float observations, followed by the seal observations, and ending with the modeling output. In section 4 we provide a broad discussion of our results along with their implications. Conclusions are in section 5.

2. Methods

2.1. Oceanographic Measurements

#### 2.1.1. On-Shelf Measurements

Four APEX profiling floats manufactured by Teledyne Webb Research were deployed in the Dalton Polynya between late December 2014 and early January 2015 from the R/V *Aurora Australis* (cruise AU1402). The floats survived up to three winters under sea ice by using a modified ice-avoidance algorithm based on Klatt et al. (2007). Profiles collected while the floats were under sea ice were stored for telemetry when ice-free conditions allowed the floats to surface. Profiles of temperature, salinity, and pressure were measured at approximately 5-day intervals, except for the first 1 to 2 weeks where the sampling interval was 1 to 2 days to check on early float progress. The Seabird SBE41CP CTD is accurate to within ± 2.4 dbar, temperature to within ± 0.002 °C, and salinity to within ± 0.01 psu, according to the manufacturer's specifications. Delayed-mode quality control procedures based on the Argo standard (Wong et al., 2018), and comparison to ship-board CTD profiles collected when the floats were deployed, confirmed that the performance of the sensors was consistent with the specifications. The floats were programmed to park on the bottom in-between profiles. In this way the drift of the floats between consecutive profiles was reduced. Pressure recorded when the floats were parked on the sea floor provided information on ocean depth. Geolocation of the profiles were recorded with a Global Positioning System fix whenever sea-ice conditions allowed the float to surface and telemeter data.

Results from the three longest-lived floats are shown here (see Figure 1). Float 1 (black in Figure 1) was deployed in the northern part of the Dalton Polynya in late December 2014 and survived one winter, collecting data for about 13 months until late January 2016. Float 1 was under sea ice between April and November 2015. Float 2 (red) was deployed further south in late December 2014 and survived for three winters. Float 2 was under sea ice for 9 months during the first winter, from April to December 2015, before surfacing and telemetering data from the winter. This float was then under sea ice continuously for 21 months from April 2016 to late November 2017 (the red star in Figure 1 indicates the position of the float when it surfaced in November 2017). Unfortunately, float 2 surfaced only once in November 2017 and it did not have enough time to transmit the data collected between February 2017 and November 2017. The float was displaced a short distance to the north between February and November 2017. Thus, float 2 provided continuous data between late December 2014 and late January 2017 (about 2 years), with known positions in the first and second summer (Figure 2). Float 3 (blue) was deployed to the south of float 2 and collected data for about 15 months, between early January 2015 and late March 2016, including 8 months under sea ice from March to December 2015. Positions have been linearly interpolated when the floats were under sea ice.

In the study we focus on the seasonality of the MCDW detected by the floats. Seasons here are defined as follows: December, January, and February as summer; March, April, and May as autumn; June, July, and August as winter; and September, October, and November as spring.

2.1.2. Off-Shelf Measurements

We use measurements from the Marine Mammals Exploring the Oceans Pole to Pole (MEOP-CTD) database (Roquet et al., 2013, 2014; see http://www.meop.net/) to characterize water properties over the continental slope. These data were collected between 2012 and 2015 by CTD-instrumented southern elephant seals (*Mirounga leonina*) on the upper slope of the Sabrina Coast (Figure 1a). Data were collected during autumn and winter months (March to July). Measurements were calibrated against historical data in nearby regions (Roquet et al., 2011). The calibrated data have estimated uncertainties of 0.02°C for temperature and 0.02 psu for practical salinity. We use data collected in a band between the 1,000-m isobath and 20 km offshore of the
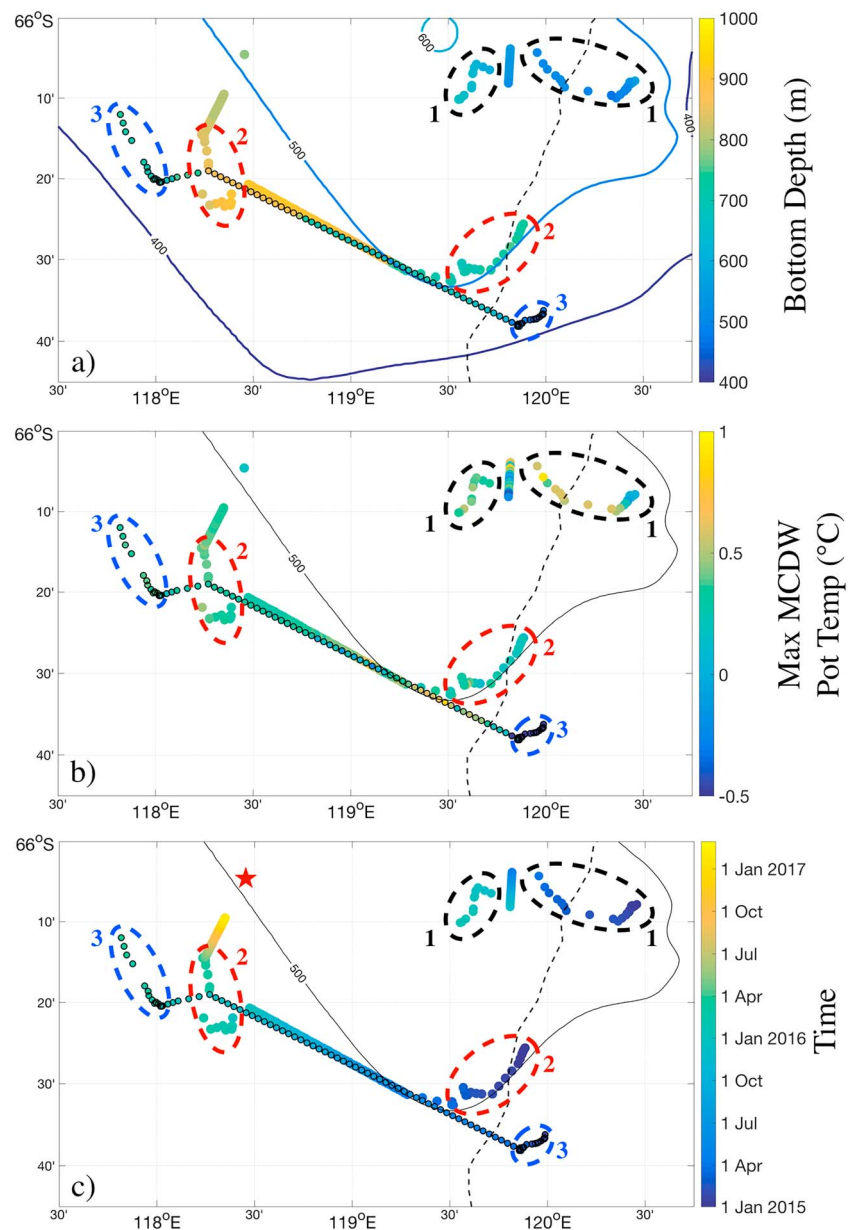
Figure 2. Float observations. (a) Bottom depth (m), (b) maximum Modified Circumpolar Deep Water (MCDW) potential temperature (°C), and (c) acquisition time for each profile collected by the floats. The black circled dots are from float 3. The area considered here is shown in Figure 1a (dashed black rectangle). Overlaid are bathymetric contours from International Bathymetric Chart of the Southern Ocean (IBCSO; Arndt et al., 2013). More depth contours are included in (a) to better compare IBCSO with float data. Measurements collected by floats 1, 2, and 3 in summer when most of the locations is known are marked by black, red, and blue dashed circles, respectively. The red star in panel (c) shows the location of the last time float 2 surfaced in November 2017. The thin dashed black line indicates the western edge of the Dalton Polynya.

1,000-m isobath in order to detect the MCDW that can potentially intrude into the depression, without being strongly affected by outflowing water from the depression. In situ observations in West Antarctica show that MCDW exiting a depression moves along isobaths shallower than 1,000 m (Zhang et al., 2016).

2.2. Ocean Model

We use monthly output from an ocean-sea ice model (Kusahara & Hasumi, 2013, 2014, Kusahara et al., 2017) to assess temporal and spatial variability of the ocean flow over the continental slope and shelf break. The

model includes ice-shelf cavities, with a fixed ice-shelf geometry. The vertical coordinate system of the ocean model is a hybrid of σ and z coordinates. The σ coordinate is applied to the uppermost three levels between the free surface and 15 m below the mean surface level to avoid vanishing of the uppermost layer thickness due to sea-ice loading and large negative amplitude of surface waves. The vertical grid spacing in the z-coordinate region is 5 m immediately below the σ coordinate and 20 m in depth range from 20 to 1,000 m. In deeper ranges of 1,000-2,000 m and 2,000-5,000 m, we use 20 vertical z-levels of 50-m and 150-m thickness, respectively. The model uses an orthogonal, curvilinear, horizontal coordinate system. Two singular points of the curvilinear coordinate are placed on the 110°E line (40 and 77°S) to regionally enhance the horizontal resolution over the East Antarctic region (see Figure S1 in the supporting information). The northern boundary of the model domain ranges from 20°S to 30°N, varying with longitude. North of 25°S, water properties (temperature and salinity) throughout the water column are restored to monthly climatology (Steele et al., 2001) with a 10-day damping timescale. The horizontal resolution in East Antarctica is less than 7 km, enabling us to resolve features of the coastline and bottom topography. The model uses IBCSO (Arndt et al., 2013) for the bathymetry over East Antarctica (56-152°E south of 60°S) and uses RTopo-1 (Timmermann et al., 2010) outside of East Antarctica. Ice-shelf draft is obtained from the RTopo-1 data set. Daily reanalysis atmospheric forcing is calculated from the ERA-Interim data set (Dee et al., 2011). The numerical model is first integrated for 10 years with 1979 forcing to spin up the ocean and sea-ice conditions, and then a hindcast simulation from 1979 to 2016 with interannually varying forcing is performed.

The numerical model adequately reproduces water masses, stratification, and currents observed on the upper slope and shelf break on the Sabrina coast (see supporting information Text S1 and Figures S2–S6). We note that most of the continental shelf has not been covered by bathymetric surveys. The modeling results are used in this study to investigate processes on the upper slope and shelf break where the IBCSO bathymetry is more reliable (Nitsche et al., 2017).

3. Results

3.1. Observations

3.1.1. Bathymetry and Circulation in the Depression

The floats were deployed on the western edge of the Dalton Polynya, where bathymetry starts to deepen on the eastern side of the depression. Float 3 was deployed in an area where the bottom depth is shallower than 500 m, while floats 1 and 2 were deployed in deeper (~500 and ~700 m, respectively) areas (Figure 2a). The maximum depth of profiles collected by floats 2 and 3 increased as the floats moved west after deployment, indicating that the floats moved into the depression (Figure 2a). Float 1 disappeared in January 2016 (Figure 2c) while still on the eastern flank of the depression at ~700-m depth (Figure 2a). Floats 2 and 3 sampled deep areas (up to ~900 m) of the depression and then reached slightly shallower areas (~800 and ~700 m, respectively; Figure 2a) before disappearing in November 2017 and March 2016, respectively (Figure 2c).

A picture of the ocean circulation in the depression is provided by the trajectories of floats 2 and 3 (Figure 2). Both trajectories indicate a cyclonic circulation as seen in other depressions around Antarctica (e.g., Assmann et al., 2013; Zhang et al., 2016). Initially, the floats moved south-westward along the eastern flank of the depression. Then, after being under sea ice between April and December 2015, they surfaced to the northwest. While the positions of profiles under sea ice are not known, the similar displacement of the two floats is consistent with cyclonic flow in the depression. Finally, the floats moved northward, again consistent with cyclonic circulation. While the floats do not fully resolve the western edge of the depression, the fact that the float furthest west (float 3) measured shallower depths than float 2 (for profiles with known positions), as well as the northward displacement of both floats, suggests that the floats reached the western flank of the depression at the end of their trajectories (Figure 2a). Positions are available for profiles collected between December 2015 and March 2016, when the floats provided new bathymetric data from the western side of the depression (Figure 2a).

3.1.2. MCDW Seasonality

MCDW was observed in all locations and at all times by the floats (Figure 2). In terms of spatial variability, the floats collected measurements in deep (>500 m) areas of the depression where MCDW was typically warmer than 0°C (Figure 2b). The only exception stems from initial measurements collected by float 3 in shallow areas (<500 m) of the polynya where MCDW was cooler (Figure 2b; see also Silvano et al., 2017, for more
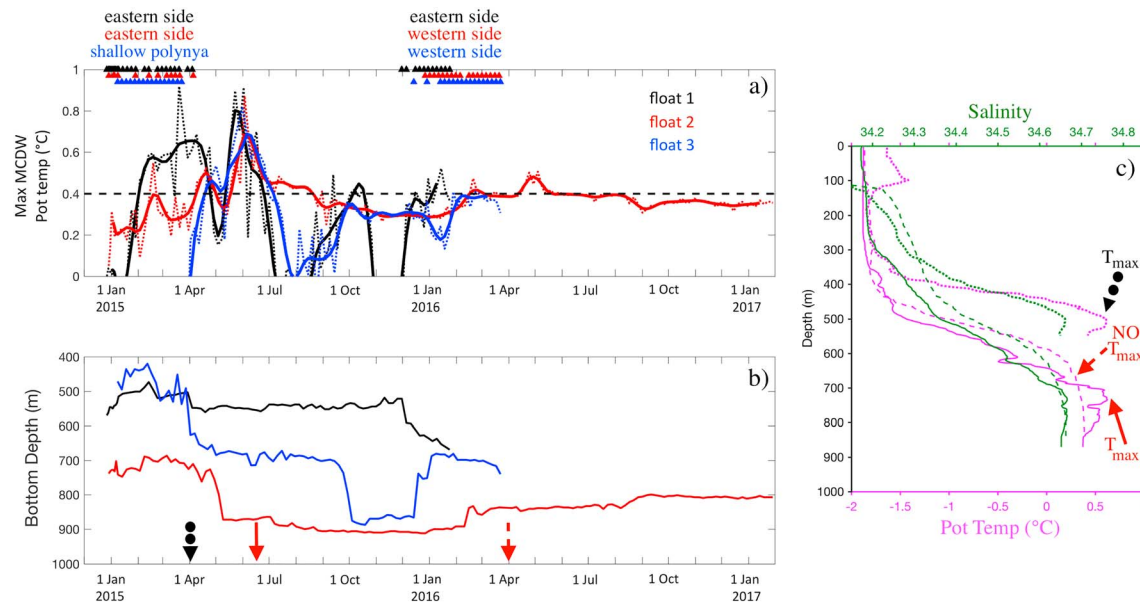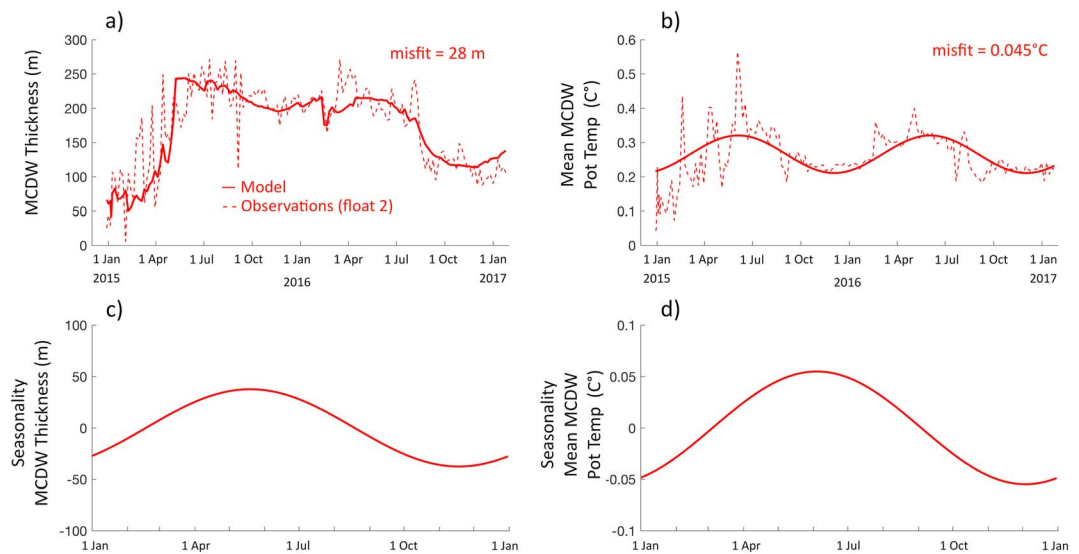
Figure 3. Modified Circumpolar Deep Water (MCDW) properties. (a) Time series of maximum MCDW potential temperature (°C) measured by float 1 (black), float 2 (red), and float 3 (blue). Values below 0°C are not included. The thick solid lines show low-pass filtered data with a 30-day fourth-order Butterworth filter, while the dotted lines show the raw data. The dashed black line shows the 0.4°C contour, which approximately separates "warmer" and "cooler" intrusions. Times when floats surfaced are indicated by the triangles along with their location (i.e., eastern/western side of the depression and shallow areas in the polynya). (b) Bottom depth as recorded by the floats. (c) Example vertical profiles of potential temperature (magenta) and salinity (green). Times of the measurements are indicated by the arrows in (b), color-coded according to the float. Note that on the western side of the depression (dashed red arrow) the maximum in MCDW potential temperature above the seafloor (T_{max}) was absent.

details about the spatial variability of MCDW on the Sabrina Coast). In terms of temporal variability, all floats showed that the MCDW temperature in the depression was higher in autumn and early winter (up to 0.9°C in March and June) compared to the rest of the year (<0.4°C; see Figure 3a). This is consistent with few (four) ship-based vertical profiles collected on the eastern side of the depression in 2015 (see their location in Figure S2) that confirmed summer MCDW cooler than 0.4°C (see Figure 3 in Silvano et al., 2017). Occasional cooling events were observed by the floats as well as persistent oscillations, which presumably represent high-frequency variability that was unresolved by the sampling rate of 5 days (see Figure 3a). Here we focus on the seasonal signal of the MCDW properties in the depression.

Float 2 measured ocean properties in the deepest areas surveyed, providing thus the most reliable data to analyze the MCDW intrusions. The clearest seasonal signal was seen between May 2015 and February 2016 when float 2 remained in areas ~900-m deep. During this period, the warmest temperatures were recorded in June (>0.6°C), while the coolest temperatures were observed from November to January (~0.3°C). The same seasonality was observed by float 2 after February 2016, even though the signal was smoother presumably because of mixing near the bottom during the transit of MCDW around the depression to reach the western side (Venables et al., 2017). Indeed, MCDW showed a maximum in temperature above the seafloor on the eastern side and in the deepest area surveyed (see dotted and solid lines in Figure 3c for example profiles), which originates off-shelf and is associated with the subsurface maximum temperature of Circumpolar Deep Water in the Southern Ocean (e.g., Orsi et al., 1995). This maximum disappeared in profiles collected on the western flank of the depression, indicating bottom mixing (see dashed lines in Figure 3c).

The record provided by the floats (2 years) is too short to compute a climatological seasonality, and therefore, we use a regression model to better characterize the annual cycle. We reconstruct the annual cycle of the thickness and mean potential temperature of the MCDW layer using data collected by float 2, which best captured the MCDW intrusions. The 0°C isotherm well represents the top of the MCDW layer (see vertical profiles in Figure 3c), and the time variability of its depth is chosen to characterize the seasonality of the MCDW thickness. We define the mean MCDW potential temperature as the potential temperature vertically averaged between the depth of the 0°C isotherm and the bottom. We consider the mean potential

Figure 4. Modified Circumpolar Deep Water (MCDW) seasonality. Time series of (a) thickness and (b) mean potential temperature (°C) of the MCDW layer from float 2. The dashed lines are the observations, while the solid lines are modeled values (as obtained from equation (1)). Also shown is the root-mean-square error (or misfit) between observed and modeled values. Seasonality (the sum of the second and third terms in equation (1)) of the thickness and mean potential temperature of the MCDW layer are shown in (c) and (d), respectively. Note that the seasonal signal of the MCDW thickness is strongly influenced by topography, and therefore, it is not apparent from Figure 4a.

temperature of the MCDW layer in order to reduce the effect of bottom mixing in our analysis. The vertically averaged temperature provides a clear seasonal signal in both years of observations collected by float 2 (see dashed line in Figure 4b), a period that spans observations from both the eastern and western side of the depression. We use the following regression model to reproduce the observations:

$$\chi = \alpha D(t) + \beta \cos(\omega t) + \gamma \sin(\omega t) \tag{1}$$

where χ represents the modelled data (i.e., MCDW thickness and mean potential temperature), t is time, D is the bottom depth, ω is a frequency representing the annual cycle, and α, β, and γ are coefficients. This regression model aims to isolate the seasonality of the MCDW properties from the effect of varying topography that influence the observations, especially the thickness of the layer. The first term on the right-hand side of equation (1) characterizes the effect of topography. The last two terms are used to quantify the seasonal signal, and for this purpose, we use only the first harmonic (period of 1 year).

The regression model well captures the observed seasonal variability (Figures 4a and 4b). The misfit between observations and the model is relatively large compared to the seasonality (misfit ~40% of the range between minimum and maximum values in Figures 4c and 4d). The misfit is mostly due to the unresolved high-frequency variability mentioned before. The modeled MCDW layer of 2015 and 2016 is up to ~75 m thicker and ~0.11°C warmer in autumn and early winter compared to spring and summer (Figures 4c and 4d).

While the float profiles reflect both spatial and temporal variability, several lines of evidence indicate that the observed seasonality in the depression was due to temporal variability of MCDW rather than spatial variability associated with drift of the floats. (1) A general pattern of higher MCDW temperature in autumn and early winter and lower temperatures during other times was observed by all floats despite different locations (Figure 3a). 2) The seasonality in temperature was most apparent when the changes in seafloor depth during float drift were minimal (e.g., float 2 between May 2015 and February 2016, Figure 3), indicating that bathymetric gradients during the drift cannot explain the observed temporal variability at the seasonal time scale. (3) Seasonality was observed in both temperature and thickness in 2015 and 2016 by float 2 (Figure 4), a period during which the float drifted from the eastern to the western side of the depression (Figure 2).

Our analysis of the float measurements collected in 2015 and 2016 shows that MCDW was warmer and thicker in autumn and early winter, and therefore, local surface cooling during these months could not

explain the seasonality. Moreover, the seasonal variability was observed deep in the water column (>500-m depth). Spreading of glacial meltwater released by nearby ice shelves and icebergs occurs at shallower depths and therefore cannot affect the observed MCDW properties (Silvano et al., 2018). Seasonal changes in the properties of the MCDW intruding onto the continental shelf are thus a likely candidate to explain the seasonality observed by the floats. We now investigate if different off-shelf sources exist that could explain the on-shelf seasonality.

3.1.3. MCDW on the Upper Continental Slope

We now compare the MCDW properties in the depression measured by the profiling floats with the MCDW observed on the upper slope by CTD-instrumented elephant seals (see section 2). We use data from all floats collected between March 2015 and February 2016 in order to include an entire year of observations of MCDW in the depression, avoiding modification by mixing which is presumably present in data collected after February 2016 (see previous section). We find that warmer intrusions (>0.4°C) observed in autumn and early winter (March to June) had properties similar to MCDW found on the upper slope to the east of the depression (Figure 5a). The similarity was apparent on the upper slope at depths ranging from 500 to 700 m, slightly deeper than the shelf break depth of the depression (~500 m), consistent with MCDW upwelling on the upper slope. Cooler intrusions in other months resembled MCDW found on the slope to the west of the depression (Figure 5b), which is cooler than the MCDW found to the east of the depression. The resemblance was most apparent in the MCDW found at 500- to 700-m depth on the western slope, again consistent with upwelling. Warmer intrusions did not overlap with MCDW found to the west of the depression (Figure 5c), while cooler intrusions only overlapped with MCDW found to the east at ~1,000-m depth (Figure 5d), likely too deep to access the depression (Nitsche et al., 2017). Finally, float data revealed a thicker layer of MCDW on the shelf in autumn and early winter (Figure 4c), in agreement with the shallower MCDW core observed in the seal data on the upper slope to the east of the depression (Figure 6a) compared to the west (Figure 6b).

The data collected by the seals are biased toward autumn and winter. However, the difference in maximum MCDW temperature (~0.5°C) between east and west of the depression observed by the seals is also observed in summer (Figure 10 in Wakatsuchi et al., 1994). This suggests that the seal observations provide a representative indication of the MCDW that can access the depression. The combination of on-shelf measurements collected by the floats and off-shelf measurements collected by the seals suggests that warmer MCDW enters the depression from the east in autumn and early winter, and cooler MCDW enters from the west during the rest of the year. We now use a numerical model to test if this mechanism is plausible.

3.2. Modeling MCDW Intrusions

In this section we show the monthly model output between March 2015 and February 2016 to compare the modeling results with the float observations described in the previous section. In Figure 7 we show maps of potential temperature and velocity vectors at 450-m depth to capture the modeled intrusions of MCDW into the depression. We include representative monthly data of autumn (March 2015), early winter (June 2015), spring (October 2015), and summer (January 2016). Modeled intrusions are persistent and, in good agreement with our inference from observations, the warmer intrusions in autumn and early winter originate to the east of the depression, while cooler intrusions in the other seasons are from the west.

As seen in the seal observations, off-shelf MCDW in the model is warmer to the east of the depression, where the "warm core" is closer to the shelf break. However, in contrast to observations, within the modeled depression there is minimal seasonal variability in the MCDW properties. This might be due to the resolution of the model, which is not adequate to represent the temporal evolution of the properties of the intruding MCDW near the seafloor (see supporting information Text S1). Moreover, the model bathymetry is likely unrealistic at the western entrance of the depression, since it is based on the interpolation of very few measurements (Nitsche et al., 2017; see, for example, the unrealistic bathymetric "bump" centered at ~117°E, 65°S in Figure 1a). Therefore, the flow of MCDW once it enters the depression from the west cannot be well reproduced by the model.

We now show the modeled currents on the upper slope and shelf break at ~120°E, just east of the depression (Figure 8; see Figure S3 for comparison with observations at this transect). Between March and June there is a strong westward flow, the Antarctic Slope Current. During this period the westward flow extends from the surface to the bottom, except in April when a weak eastward flow near the sea floor is modeled at the shelf
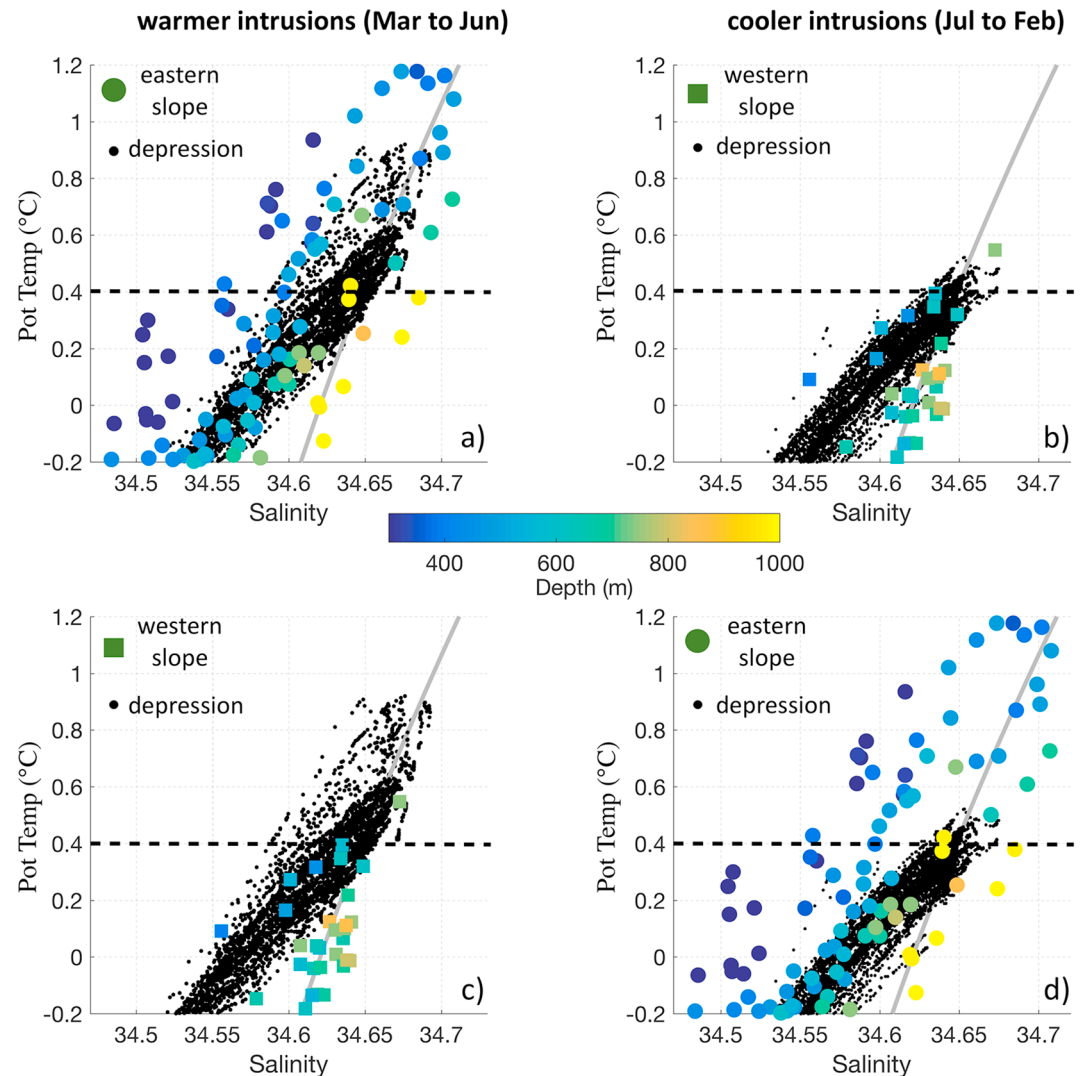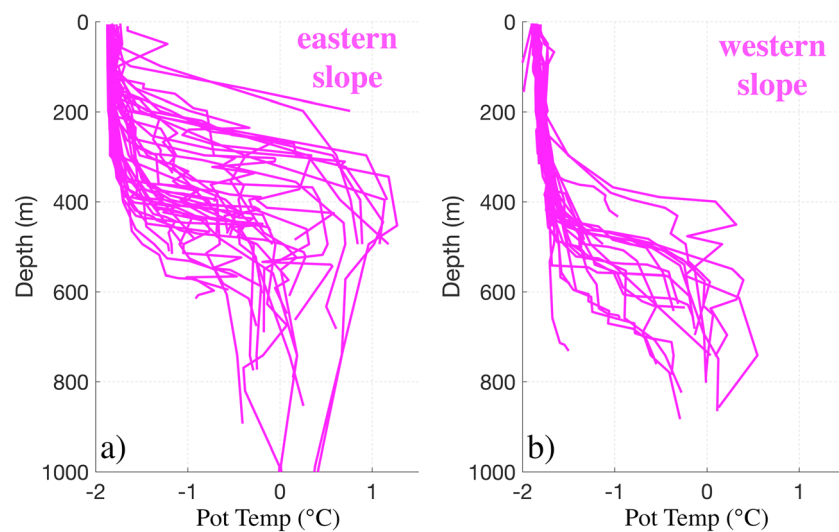
Figure 5. Sources of Modified Circumpolar Deep Water (MCDW) intrusions. The black dots are data of salinity and potential temperature (°C) collected by all floats between March 2015 and February 2016 in the depression. Float data are separated in two periods: (a and c) March to June when intrusions were warmer and (b and d) July to February when intrusions were cooler. The dashed black line shows the 0.4°C contour, which approximately separates "warmer" and "cooler" intrusions, while the 27.8 kg/m³ surface-referenced potential density contour is included in grey for reference. Seal data collected on the upper slope to the east of the depression ("eastern slope"; magenta circles in Figure 1a), color-coded according to the depth of the measurements, are superimposed in (a) and (d). Seal data collected on the upper slope to the west of the depression ("western slope"; magenta squares in Figure 1a) are shown in (b) and (c).

break. MCDW is transported in the bottom layer by the Antarctic Slope Current and is diverted into the depression at its eastern entrance (Figure 7). Between July and February the westward flow weakens and an eastward current develops on the upper slope and at the shelf break. The eastward current is faster near the seafloor, resembling the Antarctic Slope Undercurrent observed in other locations around Antarctica (e.g., Chavanne et al., 2010; Walker et al., 2013). During these months, the eastward flow at the shelf-break depth (~500 m) near the western entrance of the depression (see ocean currents at 115°E in Figure 9) allows MCDW to enter the depression from the west (Figure 7).

4. Discussion

Our study presents new bathymetric and year-round hydrographic measurements collected in deep (up to 900 m), sea-ice covered areas of the depression located on the continental shelf of the Sabrina Coast. The

Figure 6. Modified Circumpolar Deep Water (MCDW) on the upper slope. (a) Vertical profiles of potential temperature (°C) collected by conductivity-temperature-depth-instrumented seals on the upper slope to the east of the depression (eastern slope; magenta circles in Figure 1a). (b) Vertical profiles collected on the upper slope to the west of the depression (western slope; magenta squares in Figure 1a).

observations were collected by profiling floats, highlighting their ability to collect essential measurements in the sea-ice zone for multiple years not only offshore of the shelf break (e.g., Wong & Riser, 2011; Williams et al., 2011) but also on the continental shelf. These floats are therefore an important tool to better understand the influence of the ocean on melting of the Antarctic Ice Sheet.

### 4.1. Impact of Bathymetry on MCDW Delivery to Ice Shelves

The depression on the Sabrina Coast is ~500 m deep and >100 km wide at the shelf break, providing access of MCDW to the continental shelf (Nitsche et al., 2017). The depression is most likely the result of the grounded ice sheet flowing across the continental shelf in the past (Fernandez et al., 2018; Nitsche et al., 2017), as confirmed by its deepening (reaching at least 900-m depth) poleward of the shelf break. Current bathymetric products either do not capture the depression of the Sabrina Coast (e.g., Bedmap2, Fretwell et al., 2013; Nitsche et al., 2017) or, if they do, the depression is too shallow (e.g., the IBCSO product shows a maximum depth of 600 m compared to the observed values of ~900 m; see Figure 2a; Arndt et al., 2013; Silvano et al., 2017; Fernandez et al., 2018). Recent ship surveys covered only a limited portion of the Sabrina Coast (Fernandez et al., 2018; Nitsche et al., 2017; Silvano et al., 2017), and the float data used here provide limited new measurements on the western side of the depression. Future bathymetric campaigns are needed to complete the coverage of the depression and of the entire continental shelf of the Sabrina Coast.

Previous bathymetric and oceanographic data collected in summer 2015 at the front of Totten Ice Shelf revealed that two narrow (<5 km) deep (900 and 1,100 m) troughs are the main pathways for MCDW into the ice-shelf cavity (Rintoul et al., 2016). However, the measured MCDW was about -0.4°C at the Totten front, much cooler than the MCDW observed year-round in the depression (>0°C). Similar narrow troughs are present in front of the Moscow University Ice Shelf (Fernandez et al., 2018), with even cooler (-1.3°C) water sampled there (Silvano et al., 2017). These results imply that uncharted bathymetric barriers, like sills or steep slopes near the coast, prevented the warmest MCDW found in the depression from reaching the Totten and Moscow University ice shelves at the time of the summer survey (Fernandez et al., 2018; Nitsche et al., 2017; Silvano et al., 2017). Thus, MCDW and water from the thermocline above the depth of the bathymetric barriers can reach the ice-shelf cavities, while the deeper and warmer MCDW flows cyclonically and turns offshore along the western side of the depression, as suggested by the float trajectories. We argue that uncharted bathymetric features between the large depression sampled by the floats on the open continental shelf and the several narrow troughs found at the ice-shelf front likely regulate the ocean heat available to drive present and future basal melt of the Totten and Moscow University ice shelves.
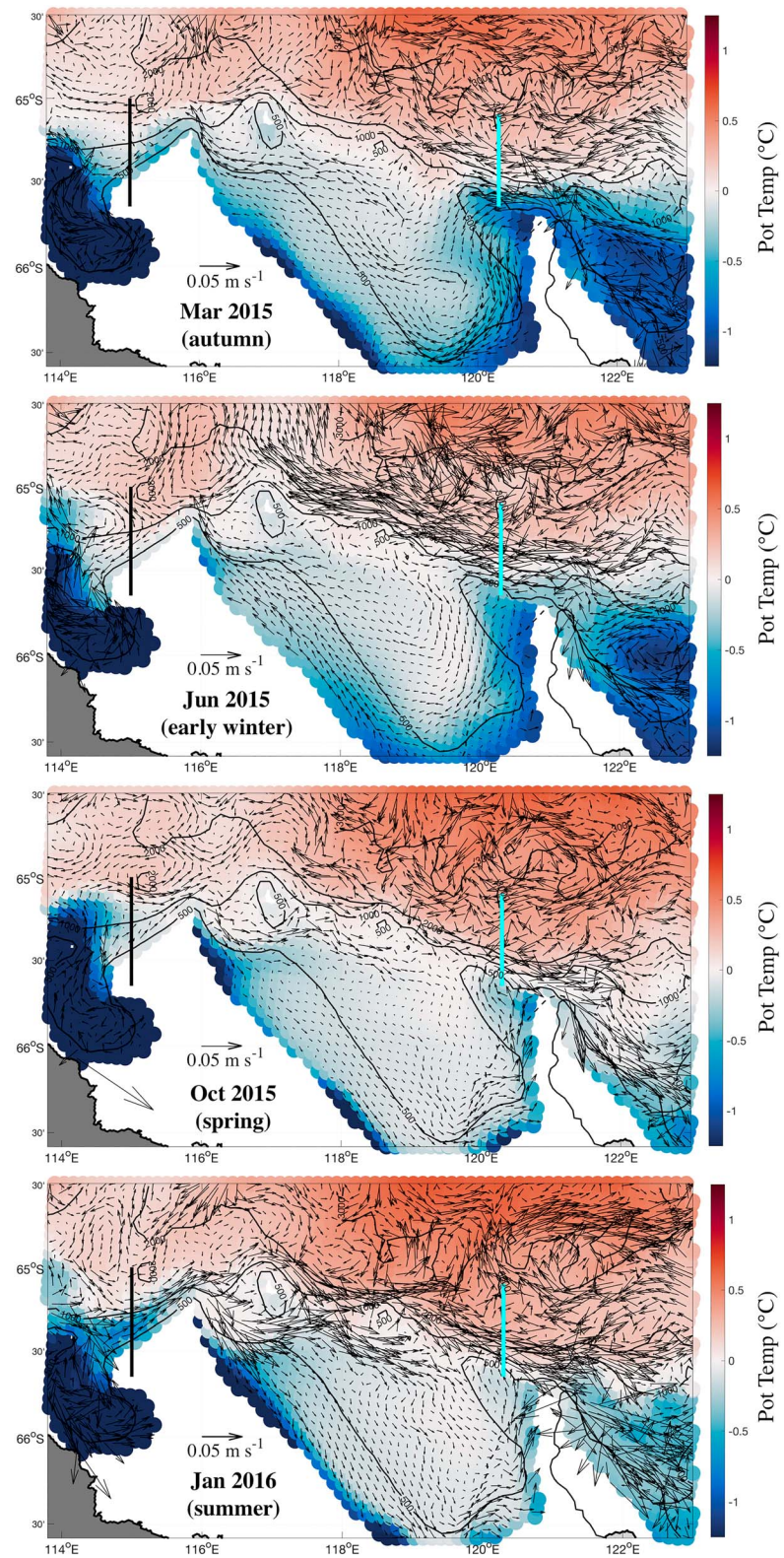
Figure 7. Modeled Modified Circumpolar Deep Water (MCDW) intrusions. Potential temperature (°C, color) and velocity (vectors) at 450-m depth in March 2015 (autumn), June 2015 (early winter), October 2015 (spring), and January 2016 (summer) from the monthly model output. The solid cyan (black) line in the panels indicates the location of the transect shown in Figure 8 (Figure 9). The white areas are shallower than 450 m in the model bathymetry (International Bathymetric Chart of the Southern Ocean (IBCSO), Arndt et al., 2013).
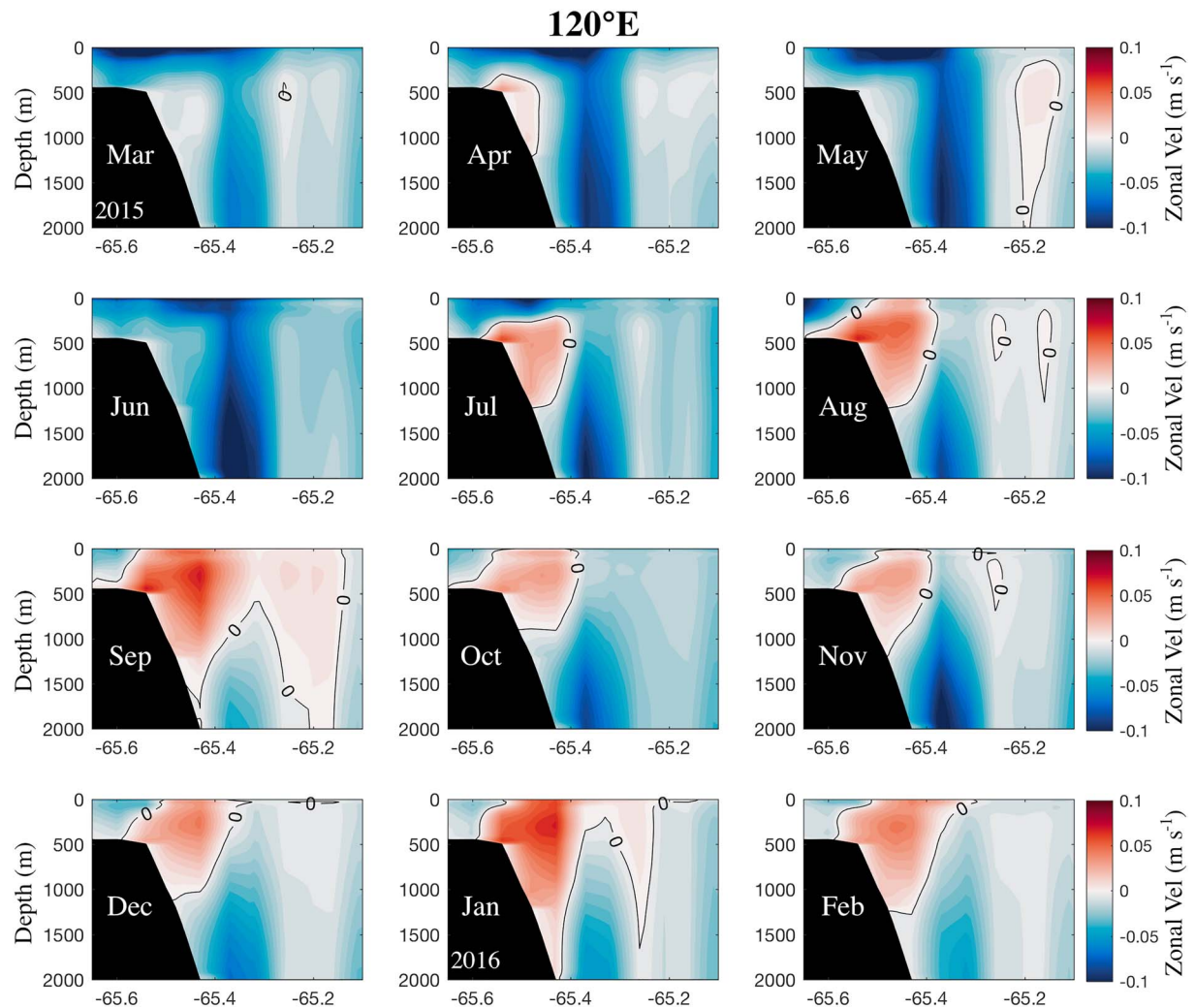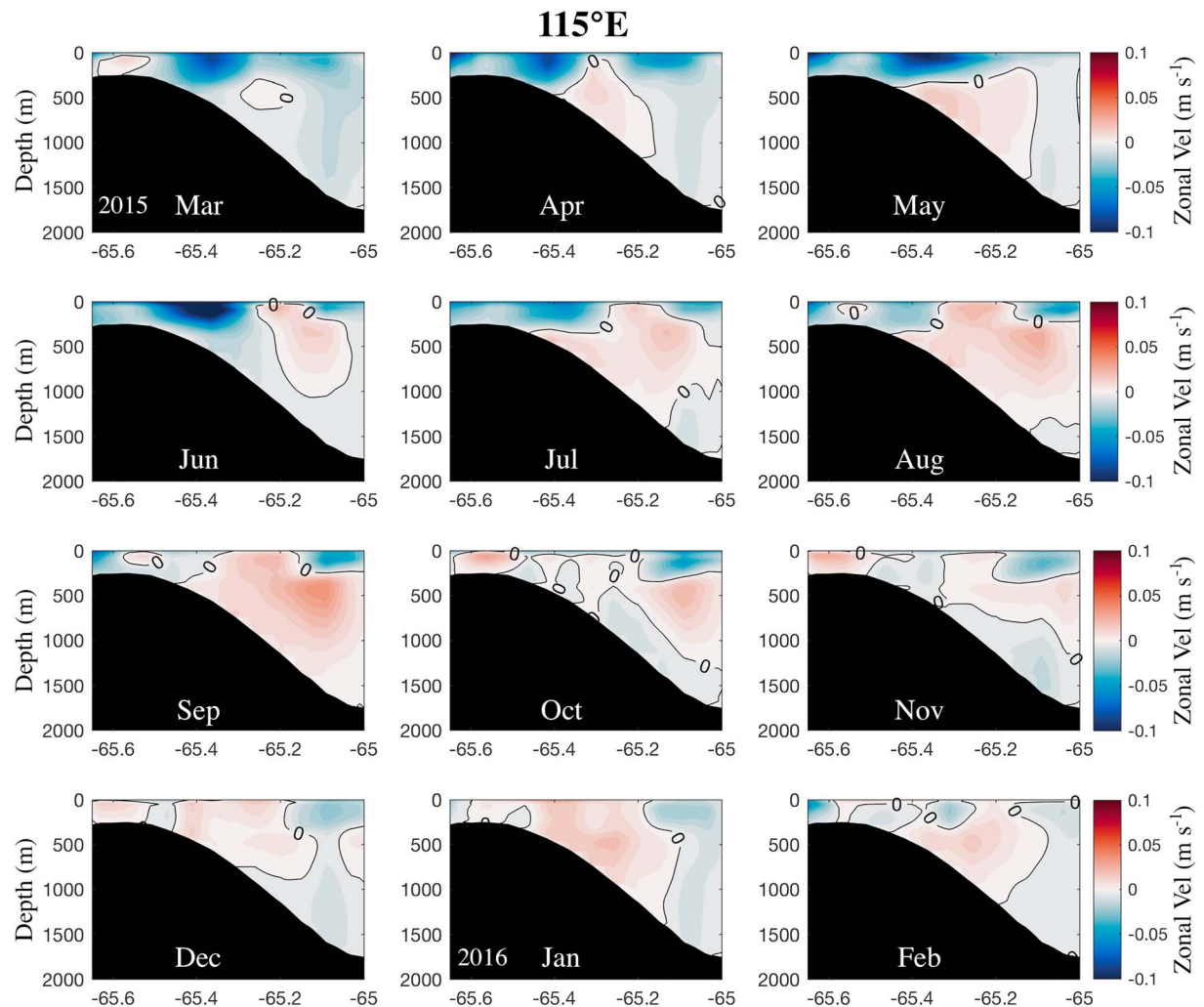
Figure 8. Modeled flow on the slope at 120°E. Zonal velocity (m/s, color) between March 2015 and February 2016 from the monthly model output at ~120°E (see cyan line in Figure 7 for location). Positive is eastward. The black line is the contour of 0 m/s.

The inferred bathymetric barriers distinguish the Sabrina Coast from the Amundsen and Bellingshausen seas, where wide, deep troughs provide a direct pathway for MCDW between the shelf break and the cavities beneath several ice shelves (Jacobs et al., 2012; Jenkins & Jacobs, 2008). Therefore, the water reaching the ice shelves in these regions is typically warmer than observed on the Sabrina Coast (Jacobs et al., 2012). The presence of a sill beneath an ice shelf can reduce the temperature of the water reaching the deepest areas of the cavity, as seen at Pine Island Glacier in the Amundsen Sea where the "reduction" is of the order of a few tenths of a degree (Dutrieux et al., 2014; Jenkins et al., 2010). The reduction observed on the Sabrina Coast (>0.7°C) is greater than that beneath Pine Island Glacier, and we argue that this may be due to uncharted bathymetric obstacles on the open continental shelf.

4.2. Seasonal Variability of MCDW Intrusions

The measurements collected in 2015 and 2016 by the floats show that the MCDW layer in the depression in autumn and early winter was ~0.11°C warmer and ~75 m thicker than in spring and summer. In terms of maximum temperature, the MCDW reached peaks of 0.9°C during autumn and early winter, while it remained below 0.4°C in other months. The observed seasonality in the depression can then affect the seasonality of the basal melt at the Totten and Moscow University ice shelves. Ocean heat delivery to the ice shelves depends not only on the properties of the MCDW accessing the continental shelf but also on temporal variability of thermocline depth near the ice shelves. Ekman pumping (Dutrieux et al., 2014; Kim

Figure 9. Modeled flow on the slope at 115°E. Zonal velocity (m/s, color) between March 2015 and February 2016 from the monthly model output at 115°E (see black line in Figure 7 for location). Positive is eastward. The black line is the contour of 0 m/s.

et al., 2017) and buoyancy forcing (Gwyther et al., 2014; Khazendar et al., 2013; St-Laurent et al., 2015) influence the thermocline depth on seasonal and interannual time scales. Unfortunately, the lack of year-round measurements at the front of ice shelves and the mostly unknown bathymetry of the Sabrina Coast prevent us from assessing the interplay between these processes using either observations or models.

The observed seasonal changes in the depression reflected different origins of MCDW reaching the continental shelf. Warmer and thicker intrusions of MCDW originated on the upper slope to the east of the depression, while cooler and thinner intrusions originated to the west. The seasonality of the flow on the upper slope explains how different MCDW sources can enter the depression at different times. In autumn and early winter a strong, top-to-bottom westward current (the Antarctic Slope Current) transports the warmer and thicker layer of MCDW from the east into the depression following isobaths. During other months, an eastward current develops near the sea floor (the Antarctic Slope Undercurrent), allowing intrusions of the cooler and thinner layer of MCDW from the west of the depression.

The MCDW is cooler on the slope to the west of the depression due to the presence of a ridge centered at ~115°E (see Figure 1a). The ridge causes cyclonic recirculation and mixing of cooler water found on the slope with offshore warm water, allowing the formation of a cooler version of MCDW at ~115°E compared to further east at the eastern entrance of the depression (~120°E; Wakatsuchi et al., 1994). Moreover, the cold surface layer is deeper at 115°E than at 120°E (Wakatsuchi et al., 1994; see also Figure 6), possibly due the

cyclonic circulation, which depresses isopycnals near the shelf break. The deeper surface layer means that a thinner layer of MCDW has access to the depression in the west. Thus, the cyclonic circulation in the presence of a ridge helps explain the cooler and thinner layer of MCDW entering the depression from the west.

Observations of seasonal variability of the flow on the Antarctic slope are scarce due to the logistical issues that complicate the deployment and recovery of moorings in this region. Furthermore, the deployment of fixed instruments in the top 500 m of the water column is high risk due to the presence of drifting icebergs. Recently, estimates of the barotropic component of the flow on the Antarctic slope have been obtained through the use of satellite altimeters (Armitage et al., 2018; Dotto et al., 2018) and a few moored arrays (e.g., Núñez-Riboni & Fahrbach, 2009; Peña-Molino et al., 2016). Those estimates are consistent with the results of our model: the westward flow associated with the Antarctic Slope Current is stronger in autumn and winter while it is weaker in spring and summer. The seasonal variability of the Antarctic Slope Current is mostly driven by seasonality of the easterly winds, which are stronger in autumn and winter and weaker in spring and summer (Armitage et al., 2018; Mathiot et al., 2011; Núñez-Riboni & Fahrbach, 2009).

Ship-based observations have been used in previous studies to obtain a snapshot of the vertical structure of the flow on the upper slope and at the shelf break. Núñez-Riboni and Fahrbach (2009) provide a snapshot in all seasons in the eastern Weddell Sea. Their results are in agreement with our modeling results: top-to-bottom westward flow in autumn and winter (the Antarctic Slope Current) and the presence of an eastward current near the bottom (the Antarctic Slope Undercurrent) in spring and summer. The Antarctic Slope Undercurrent has also been observed in other summer surveys in the eastern Weddell Sea (Chavanne et al., 2010; Heywood et al., 1998) and in the Amundsen Sea (Walker et al., 2013). The mechanisms of formation of the Antarctic Slope Undercurrent are largely unknown. Some studies suggest that waves on the continental slope allow the undercurrent to form (e.g., Chavanne et al., 2010). Other studies associate the undercurrent with Ekman downwelling on the upper continental slope driven by the Easterlies (e.g., Jenkins et al., 2016). The downwelling causes southward deepening of the isopycnals and the formation of the Antarctic Slope Front. The vertical shear associated with the Antarctic Slope Front then allows the undercurrent to form in the bottom layer beneath the westward Antarctic Slope Current. Further investigation, beyond the scope of this study, is required to understand the dynamics of the Antarctic Slope Undercurrent and how it varies with time and location.

The mechanism we propose to explain the observed seasonality of the MCDW intrusions into the depression of the Sabrina Coast is consistent with the results of other studies of the flow on the Antarctic slope. Other mechanisms can also be important on seasonal time scales, including changes in the bottom Ekman boundary layer (Wåhlin et al., 2012) and deepening/shoaling of isopycnals (Årthun et al., 2012; Mallett et al., 2018) on the slope. Moreover, small-scale features on the Antarctic slope are not well resolved by our model. Therefore, processes like eddies (Stewart & Thompson, 2015), waves (St-Laurent et al., 2013), tidal fluctuations (Stewart et al., 2018), and the dynamics of jets forming on the slope (Peña-Molino et al., 2016; Thompson & Heywood, 2008) are not well captured in our study and they can influence cross-shelf exchange. Nevertheless, the consistency between observations and modeling results in our study suggests that seasonal variability of the flow on the Antarctic slope regulates the seasonality of the MCDW intrusions onto the Sabrina Coast continental shelf. Sustained year-round measurements on the slope and shelf are needed to corroborate our proposed mechanism and to better characterize seasonal variations.

5. Conclusions

Profiling floats allowed collection of 2 years of unprecedented oceanographic and bathymetric measurements in sea-ice covered areas of the Sabrina Coast continental shelf. They confirm that the deep (up to 900 m deep) depression found on the continental shelf is filled by warm (>0°C) MCDW that originated off the shelf. The warmest core of MCDW observed year-round near the sea floor in the depression has not been observed entering the ice-shelf cavities, suggesting that uncharted bathymetric barriers on the continental shelf regulate the ocean heat delivery to the Totten and Moscow University ice shelves.

Our observations in the depression revealed a warmer and thicker MCDW layer in autumn and early winter compared to spring and summer. Results from an ocean model indicate that the seasonality of the flow on the upper slope and shelf break can explain the seasonality of the MCDW observed on the shelf. In

autumn and early winter a strong westward current (the Antarctic Slope Current) promotes warm intrusions from east of the depression. In spring and summer an eastward current develops near the bottom (the Antarctic Slope Undercurrent) that allows intrusions from the west where off-shelf MCDW is cooled by a permanent cyclonic eddy.

Our study shows that changes in the flow on the Antarctic continental slope influence the temperature and thickness of the MCDW layer that can access the continental shelf and, ultimately, deliver ocean heat to the Antarctic ice shelves. Constraining future changes in the flow on the Antarctic slope driven by changes of winds (Spence et al., 2014) or sea ice (Hellmer et al., 2012) is therefore required to develop projections of mass loss from the Antarctic Ice Sheet.

References

Allen, S. E., & Durrieu de Madron, X. (2009). A review of the role of submarine canyons in deep-ocean exchange with the shelf. *Ocean Science*, *5*(4), 607–620. https://doi.org/10.5194/os-5-607-2009

Armitage, T. W. K., Kwok, R., Thompson, A. F., & Cunningham, G. (2018). Dynamic topography and sea level anomalies of the Southern Ocean: Variability and teleconnections. *Journal of Geophysical Research: Oceans*, *123*(1), 613–630. https://doi.org/10.1002/2017JC013534

Arndt, J. E., Schenke, H. W., Jakobsson, M., Nitsche, F. O., Buys, G., Goleby, B., et al. (2013). The International Bathymetric Chart of the Southern Ocean (IBCSO) version 1.0—A new bathymetric compilation covering circum-Antarctic waters. *Geophysical Research Letters*, *40*, 3111–3117. https://doi.org/10.1002/grl.50413

Årthun, M., Nicholls, K. W., Makinson, K., Fedak, M. A., & Boehme, L. (2012). Seasonal inflow of warm water onto the southern Weddell Sea continental shelf, Antarctica. *Geophysical Research Letters*, *39*, L17601. https://doi.org/10.1029/2012GL052856

Assmann, K. M., Jenkins, A., Shoosmith, D. R., Walker, D. P., Jacobs, S. S., & Nicholls, K. W. (2013). Variability of Circumpolar Deep Water transport onto the Amundsen Sea continental shelf through a shelf break trough. *Journal of Geophysical Research: Oceans*, *118*, 6603–6620. https://doi.org/10.1002/2013JC008871

Bindoff, N. L., Rosenberg, M. A., & Warner, M. J. (2000). On the circulation and water masses over the Antarctic continental slope and rise between 80 and 150°E. *Deep-Sea Research, Part II*, *47*(12–13), 2299–2326. https://doi.org/10.1016/S0967-0645(00)00038-2

Chavanne, C. P., Heywood, K. J., Nicholls, K. W., & Fer, I. (2010). Observations of the Antarctic Slope Undercurrent in the southeastern Weddell Sea. *Geophysical Research Letters*, *37*, L13601. https://doi.org/10.1029/2010GL043603

Christianson, K., Bushuk, M., Dutrieux, P., Parizek, B. R., Joughin, I. R., Alley, R. B., et al. (2016). Sensitivity of pine island glacier to observed ocean forcing. *Geophysical Research Letters*, *43*, 10,817–10,825. https://doi.org/10.1002/2016GL070500

Darelius, E., Fer, I., & Nicholls, K. W. (2016). Observed vulnerability of Filchner-Ronne Ice Shelf to wind-driven inflow of warm deep water. *Nature Communications*, *7*, 12300. https://doi.org/10.1038/ncomms12300

Dee, D. P., Uppala, S. M., Simmons, A. J., Berrisford, P., Poli, P., Kobayas, S., et al. (2011). The ERA-Interim reanalysis: Configuration and performance of the data assimilation system. *Quarterly Journal of the Royal Meteorological Society*, *137*(656), 553–597. https://doi.org/10.1002/qj.828

Dinniman, M. S., Klinck, J. M., Hofmann, E. E., & Smith, W. O. Jr. (2018). Effects of projected changes in wind, atmospheric temperature, and freshwater inflow on the Ross Sea. *Journal of Climate*, *31*(4), 1619–1635. https://doi.org/10.1175/JCLI-D-17-0351.s1

Dinniman, M. S., Klinck, J. M., & Smith, W. O. Jr. (2003). Cross-shelf exchange in a model of the Ross Sea circulation and biogeochemistry. *Deep-Sea Research, Part II*, *50*(22-26), 3103–3120. https://doi.org/10.1016/j.dsr2.2003.07.011

Dotto, T. S., Naveira Garabato, A., Bacon, S., Tsamados, M., Holland, P. R., Hooley, J., et al. (2018). Variability of the Ross Gyre, Southern Ocean: Drivers and responses revealed by satellite altimetry. *Geophysical Research Letters*, *45*, 6195–6204. https://doi.org/10.1029/2018GL078607

Dutrieux, P., De Rydt, J., Jenkins, A., Holland, P. R., Ha, H. K., Lee, S. H., et al. (2014). Strong sensitivity of Pine Island ice-shelf melting to climatic variability. *Science*, *343*(6167), 174–178. https://doi.org/10.1126/science.1244341

Fernandez, R., Gulick, S., Domack, E., Montelli, S., Leventer, A., Shevenell, A., & Frederick, B. (2018). Past ice stream and ice sheet changes on the continental shelf off the Sabrina Coast, East Antarctica. *Geomorphology*, *317*, 10–22. https://doi.org/10.1016/j.geomorph.2018.05.020

Fretwell, P., Pritchard, H. D., Vaughan, D. G., Bamber, J. L., Barrand, N. E., Bell, R., et al. (2013). Bedmap2: Improved ice bed, surface and thickness datasets for Antarctica. *The Cryosphere*, *7*(1), 375–393. https://doi.org/10.5194/tc-7-375-2013

Gille, S. T., McKee, D. C., & Martinson, D. G. (2016). Temporal changes in the Antarctic Circumpolar Current: Implications for the Antarctic continental shelves. *Oceanography*, *29*(4), 96–105. https://doi.org/10.5670/oceanog.2016.102

Greenbaum, J. S., Blankenship, D. D., Young, D. A., Richter, T. G., Roberts, J. L., Aitken, A. R. A., et al. (2015). Ocean access to a cavity beneath Totten Glacier in East Antarctica. *Nature Geoscience*, *8*(4), 294–298. https://doi.org/10.1038/ngeo2388

Greene, C. A., Blankenship, D. D., Gwyther, D. E., Silvano, A., & van Wijk, E. (2017). Wind causes Totten Ice Shelf melt and acceleration. *Science Advances*, *3*(11), e1701681. https://doi.org/10.1126/sciadv.1701681

Gulick, S. P. S., Montelli, A., Shevenell, A., Fernandez, R., Smith, C., Warny, S., et al. (2017). Initiation and long-term instability of the East Antarctic Ice Sheet. *Nature*, *552*(7684), 225–229. https://doi.org/10.1038/nature25026

Gwyther, D. E., Galton-Fenzi, B. K., Hunter, J. R., & Roberts, J. L. (2014). Simulated melt rates for the Totten and Dalton ice shelves. *Ocean Science*, *10*(3), 267–279. https://doi.org/10.5194/os-10-267-2014

Harig, C., & Simons, F. J. (2015). Accelerated West Antarctic ice mass loss continues to outpace East Antarctic gains. *Earth and Planetary Science Letters*, *415*, 134–141. https://doi.org/10.1016/j.epsl.2015.01.029

Hellmer, H. H., Kauker, F., Timmermann, R., Determann, J., & Rae, J. (2012). Twenty-first-century warming of a large Antarctic ice-shelf cavity by a redirected coastal current. *Nature*, *485*(7397), 225–228. https://doi.org/10.1038/nature11064

Heywood, K. J., Locarnini, R. A., Frew, R. D., Dennis, P. F., & King, B. A. (1998). Transport and water masses of the Antarctic Slope Front system in the eastern Weddell Sea. In S. S. Jacobs & R. F. Weiss (Eds.), *Ocean, Ice and Atmosphere: Interactions at the Antarctic Continental Margin, Antarctic Research Series* (Vol. 75, pp. 203–214). Washington, DC: American Geophysical Union. https://doi.org/10.1029/AR075p0203

Jacobs, S., Jenkins, A., Hellmer, H., Giulivi, C., Nitsche, F., Huber, B., & Guerrero, R. (2012). The Amundsen Sea and the Antarctic ice sheet. *Oceanography*, *25*(3), 154–163. https://doi.org/10.5670/oceanog.2012.90

Jenkins, A., Dutrieux, P., Jacobs, S., Steig, E. J., Gudmundsson, G. H., Smith, J., & Heywood, K. J. (2016). Decadal ocean forcing and Antarctic ice sheet response: Lessons from the Amundsen Sea. *Oceanography*, *29*(4), 106–117. https://doi.org/10.5670/oceanog.2016.103

Jenkins, A., Dutrieux, P., Jacobs, S. S., McPhail, S. D., Perrett, J. R., Webb, A. T., & White, D. (2010). Observations beneath Pine Island Glacier in West Antarctica and implications for its retreat. *Nature Geoscience*, *3*(7), 468–472. https://doi.org/10.1038/ngeo890

Jenkins, A., & Jacobs, S. S. (2008). Circulation and melting beneath George VI ice shelf, Antarctica. *Journal of Geophysical Research*, *113*(C4), C04013. https://doi.org/10.1029/2007JC004449

Khazendar, A., Schodlok, M. P., Fenty, I., Ligtenberg, S. R. M., Rignot, E., & van den Broeke, M. R. (2013). Observed thinning of Totten Glacier is linked to coastal polynya variability. *Nature Communications*, *4*(1). https://doi.org/10.1038/ncomms3857

Kim, T. W., Ha, H. K., Wåhlin, A. K., Lee, S. H., Kim, C. S., Lee, J. H., & Cho, Y. K. (2017). Is Ekman pumping responsible for the seasonal variation of warm circumpolar deep water in the Amundsen Sea? *Continental Shelf Research*, *132*, 38–48. https://doi.org/10.1016/j.csr.2016.09.005

Klatt, O., Boebel, O., & Fahrbach, E. (2007). A profiling float's sense of ice. *Journal of Atmospheric and Oceanic Technology*, *24*(7), 1301–1308. https://doi.org/10.1175/JTECH2026.1

Klinck, J. M. (1996). Circulation near submarine canyons: A modeling study. *Journal of Geophysical Research*, *101*(C1), 1211–1223. https://doi.org/10.1029/95JC02901

Kohut, J., Hunter, E., & Huber, B. (2013). Small-scale variability of the cross-shelf flow over the outer shelf of the Ross Sea. *Journal of Geophysical Research: Oceans*, *118*, 1863–1876. https://doi.org/10.1002/jgrc.20090

Kusahara, K., & Hasumi, H. (2013). Modeling Antarctic ice shelf responses to future climate changes and impacts on the ocean. *Journal of Geophysical Research: Oceans*, *118*, 2454–2475. https://doi.org/10.1002/jgrc.20166

Kusahara, K., & Hasumi, H. (2014). Pathways of basal meltwater from Antarctic ice shelves: A model study. *Journal of Geophysical Research: Oceans*, *119*, 5690–5704. https://doi.org/10.1002/2014JC009915

Kusahara, K., Hasumi, H., Fraser, A. D., Aoki, S., Shimada, S., Williams, G. D., et al. (2017). Modeling ocean-cryosphere interactions off Adélie and George V Land, East Antarctica. *Journal of Climate*, *30*(1), 163–188. https://doi.org/10.1175/JCLI-D-15-0808.1

Li, X., Rignot, E., Mouginot, J., & Scheuchl, B. (2016). Ice flow dynamics and mass loss of Totten Glacier, East Antarctica from 1989 to 2015. *Geophysical Research Letters*, *43*, 6366–6373. https://doi.org/10.1002/2016GL069173

Mallett, H. K. W., Boehme, L., Fedak, M., Heywood, K. J., Stevens, D. P., & Roquet, F. (2018). Variation in the distribution and properties of circumpolar deep water in the eastern Amundsen Sea, on seasonal timescales, using seal-borne tags. *Geophysical Research Letters*, *45*(10), 4982–4990. https://doi.org/10.1029/2018GL077430

Marshall, J., & Speer, K. (2012). Closure of the meridional overturning circulation through Southern Ocean upwelling. *Nature Geoscience*, *5*(3), 171–180. https://doi.org/10.1038/ngeo1391

Mathiot, P., Goosse, H., Fichefet, T., Barnier, B., & Gall ee, H. (2011). Modelling the seasonal variability of the Antarctic Slope Current. *Ocean Science*, *7*(4), 455–470. https://doi.org/10.5194/os-7-455-2011

Moffat, C., Owens, B., & Beardsley, R. C. (2009). On the characteristics of Circumpolar Deep Water intrusions to the west Antarctic Peninsula Continental Shelf. *Journal of Geophysical Research*, *114*(C5), C05017. https://doi.org/10.1029/2008JC004955

Mohajerani, Y., Velicogna, I., & Rignot, E. (2018). Mass loss of Totten and Moscow University glaciers, East Antarctica, using regionally optimized GRACE mascons. *Geophysical Research Letters*, *45*(14), 7010–7018. https://doi.org/10.1029/2018GL078173

Nitsche, F. O., Porter, D., Williams, G., Cougnon, E. A., Fraser, A. D., Correia, R., & Guerrero, R. (2017). Bathymetric control of warm ocean water access along the East Antarctic Margin. *Geophysical Research Letters*, *44*, 8936–8944. https://doi.org/10.1002/2017GL074433

Nøst, O. A., Biuw, M., Tverberg, V., Lydersen, C., Hattermann, T., Zhou, Q., et al. (2011). Eddy overturning of the Antarctic Slope Front controls glacial melting in the Eastern Weddell Sea. *Journal of Geophysical Research*, *116*, C11014. https://doi.org/10.1029/2011JC006965

Núñez-Riboni, I., & Fahrbach, E. (2009). Seasonal variability of the Antarctic Coastal Current and its driving mechanisms in the Weddell Sea. *Deep-Sea Research, Part I*, *56*(11), 1927–1941. https://doi.org/10.1016/j.dsr.2009.06.005

Orsi, A. H., Whitworth, T., & Nowlin, W. D. (1995). On the meridional extent and fronts of the Antarctic Circumpolar Current. *Deep-Sea Research, Part I*, *42*(5), 641–673. https://doi.org/10.1016/0967-0637(95)00021-W

Orsi, A. H., & Wiederwohl, C. L. (2009). A recount of Ross Sea waters. *Deep-Sea Research, Part II*, *56*(13–14), 778–795. https://doi.org/10.1016/j.dsr2.2008.10.033

Palóczy, A., Gille, S. T., & McClean, J. L. (2018). Oceanic heat delivery to the Antarctic continental shelf: Large-scale, low-frequency variability. *Journal of Geophysical Research: Oceans*, *123*(11), 7678–7701. https://doi.org/10.1029/2018JC014345

Peña-Molino, B., McCartney, M. S., & Rintoul, S. R. (2016). Direct observations of the Antarctic Slope Current transport at 1138E. *Journal of Geophysical Research: Oceans*, *121*, 7390–7407. https://doi.org/10.1002/2015JC011594

Pritchard, H. D., Ligtenberg, S. R. M., Fricker, H. A., Vaughan, D. G., van den Broeke, M. R., & Padman, L. (2012). Antarctic ice–sheet loss driven by basal melting of ice shelves. *Nature*, *484*(7395), 502–505. https://doi.org/10.1038/nature10968

Rignot, E., Bamber, J. L., Van Den Broeke, M. R., Davis, C., Li, Y., Van Den Berg, W. J., & Van Meijgaard, E. (2008). Recent Antarctic ice mass loss from radar interferometry and regional climate modelling. *Nature Geoscience*, *1*(2), 106–110. https://doi.org/10.1038/ngeo102

Rintoul, S., & Naveira Garabato, A. C. (2013). Dynamics of the Southern Ocean circulation. In J. G. G. Siedler, et al. (Eds.), *Ocean Circulation and Climate: A 21st Century Perspective, International Geophysics Series* (Vol. 103, pp. 471–492). N. Y: Elsevier. https://doi.org/10.1016/B978-0-12-391851-2.00018-0

Rintoul, S. R. (2018). The global influence of localized dynamics in the Southern Ocean. *Nature*, *558*(7709), 209–218. https://doi.org/10.1038/s41586-018-0182-3

Rintoul, S. R., Silvano, A., Peña-Molino, B., van Wijk, E., Rosenberg, M. A., Greenbaum, J. S., & Blankenship, D. D. (2016). Ocean heat drives rapid basal melt of Totten Ice Shelf. *Science Advances*, *2*(12), e1601610. https://doi.org/10.1126/sciadv.1601610

Roberts, J., Galton-Fenzi, B. K., Paolo, F. S., Donnelly, C., Gwyther, D. E., Padman, L., et al. (2017). *Ocean forced variability of Totten Glacier mass loss*, Special Publications (Vol. *461*, pp. 175–186). London: Geological Society. https://doi.org/10.1144/SP461.6

Roquet, F., Charrassin, J. B., Marchand, S., Boehme, L., Fedak, M., Reverdin, G., & Guinet, C. (2011). Delayed-mode calibration of hydrographic data obtained from animal-borne satellite relay data loggers. *Journal of Atmospheric and Oceanic Technology*, *28*(6), 787–801. https://doi.org/10.1175/2010JTECHO801.1

Roquet, F., Williams, G., Hindell, M. A., Harcourt, R., McMahon, C., Guinet, C., et al. (2014). A southern Indian Ocean database of hydrographic profiles obtained with instrumented elephant seals. *Scientific Data*, *1*, 140028. https://doi.org/10.1038/sdata.2014.28

Roquet, F., Wunsch, C., Forget, G., Heimbach, P., Guinet, C., Reverdin, G., et al. (2013). Estimates of the Southern Ocean general circulation improved by animal-borne instruments. *Geophysical Research Letters*, *40*, 6176–6180. https://doi.org/10.1002/2013GL058304

Scambos, T., Bohlander, J., & Raup, B. (1996). Images of Antarctic Ice Shelves [2002-present], Boulder, Colorado USA: National Snow and Ice Data Center. https://doi.org/10.7265/N5NC5Z4N.

Scambos, T. A., Bohlander, J. A., Shuman, C. A., & Skvarca, P. (2004). Glacier acceleration and thinning after ice shelf collapse in the Larsen B embayment, Antarctica. *Geophysical Research Letters*, *31*, L18402. https://doi.org/10.1029/2004GL020670

Shepherd, A., Ivins, E., Rignot, E., Smith, B., van den Broeke, M., Velicogna, I., et al. (2018). Mass balance of the Antarctic Ice Sheet from 1992 to 2017. *Nature*, *558*(7709), 219–222. https://doi.org/10.1038/s41586-018-0179-y

Silvano, A., Rintoul, S. R., & Herraiz-Borreguero, L. (2016). Ocean-ice shelf interaction in East Antarctica. *Oceanography*, *29*(4), 130–143. https://doi.org/10.5670/oceanog.2016.105

Silvano, A., Rintoul, S. R., Peña-Molino, B., Hobbs, W. R., van Wijk, E., Aoki, S., et al. (2018). Freshening by glacial meltwater enhances melting of ice shelves and reduces formation of Antarctic Bottom Water. *Science Advances*, *4*(4), eaap9467. https://doi.org/10.1126/sciadv.aap9467

Silvano, A., Rintoul, S. R., Peña-Molino, B., & Williams, G. D. (2017). Distribution of water masses and meltwater on the continental shelf near the Totten and Moscow University ice shelves. *Journal of Geophysical Research: Oceans*, *122*, 2050–2068. https://doi.org/10.1002/2016JC012115

Spence, P., Griffies, S. M., England, M. H., Hogg, A. M., Saenko, O. A., & Jourdain, N. C. (2014). Rapid subsurface warming and circulation changes of Antarctic coastal waters by poleward shifting winds. *Geophysical Research Letters*, *41*, 4601–4610. https://doi.org/10.1002/2014GL060613

Steele, M., Morley, R., & Ermold, W. (2001). PHC: A global ocean hydrography with a high quality Arctic Ocean. *Journal of Climate*, *14*(9), 2079–2087. https://doi.org/10.1175/1520-0442(2001)014<2079:PAGOHW>2.0.CO;2

Stewart, A. L., Klocker, A., & Menemenlis, D. (2018). Circum-Antarctic shoreward heat transport derived from an eddy- and tide-resolving simulation. *Geophysical Research Letters*, *45*(2), 834–845. https://doi.org/10.1002/2017GL075677

Stewart, A. L., & Thompson, A. F. (2015). Eddy-mediated transport of warm Circumpolar Deep Water across the Antarctic Shelf Break. *Geophysical Research Letters*, *42*, 432–440. https://doi.org/10.1002/2014GL062281

St-Laurent, P., Klinck, J. M., & Dinniman, M. S. (2013). On the role of coastal troughs in the circulation of warm circumpolar deep water on Antarctic Shelves. *Journal of Physical Oceanography*, *43*(1), 51–64. https://doi.org/10.1175/JPO-D-11-0237.1

St-Laurent, P., Klinck, J. M., & Dinniman, M. S. (2015). Impact of local winter cooling on the melt of Pine Island Glacier, Antarctica. *Journal of Geophysical Research: Oceans*, *120*, 6718–6732. https://doi.org/10.1002/2015JC010709

Thompson, A. F., & Heywood, K. J. (2008). Frontal structure and transport in the northwestern Weddell Sea. *Deep-Sea Research, Part I*, *55*(10), 1229–1251. https://doi.org/10.1016/j.dsr.2008.06.001

Thompson, A. F., Heywood, K. J., Schmidtko, S., & Stewart, A. L. (2014). Eddy transport as a key component of the Antarctic overturning circulation. *Nature Geoscience*, *7*(12), 879–884. https://doi.org/10.1038/ngeo2289

Thompson, A. F., Stewart, A. L., Spence, P., & Heywood, K. J. (2018). The Antarctic Slope Current in a changing climate. *Reviews of Geophysics*, *56*(4), 741–770. https://doi.org/10.1029/2018RG000624

Timmermann, R., Le Brocq, A., Deen, T., Domack, E., Dutrieux, P., Galton-Fenzi, B., & Smith, W. H. F. (2010). A consistent data set of Antarctic ice sheet topography, cavity geometry, and global bathymetry. *Earth System Science Data*, *2*, 261–273. https://doi.org/10.5194/essd-2-261-2010

Velicogna, I., Sutterley, T., & van den Broeke, M. (2014). Regional acceleration in ice mass loss from Greenland and Antarctica using GRACE time-variable gravity data. *Geophysical Research Letters*, *41*, 8130–8137. https://doi.org/10.1002/2014GL061052

Venables, H. J., Meredith, M. P., & Brearley, J. A. (2017). Modification of deep waters in Marguerite Bay, western Antarctic Peninsula, caused by topographic overflows. *Deep-Sea Research, Part II*, *139*(9–17), 9–17. https://doi.org/10.1016/j.dsr2.2016.09.005

Wåhlin, A. K., Muench, R. D., Arneborg, L., Björk, G., Ha, H., Lee, S. H., & Alsén, H. (2012). Some implications of Ekman layer dynamics for cross-shelf exchange in the Amundsen Sea. *Journal of Physical Oceanography*, *42*(9), 1461–1474. https://doi.org/10.1175/JPO-D-11-041.1

Wakatsuchi, M., Ohshima, K. I., Hishida, M., & Naganobu, M. (1994). Observations of a street of cyclonic eddies in the Indian Ocean sector of the Antarctic Divergence. *Journal of Geophysical Research*, *99*(C10), 20,417–20,426. https://doi.org/10.1029/94JC01478

Walker, D. P., Jenkins, A., Assmann, K. M., Shoosmith, D. R., & Brandon, M. A. (2013). Oceanographic observations at the shelf break of the Amundsen Sea, Antarctica. *Journal of Geophysical Research: Oceans*, *118*, 2906–2918. https://doi.org/10.1002/jgrc.20212

Williams, G. D., Bindoff, N. L., Marsland, S. J., & Rintoul, S. R. (2008). Formation and export of dense shelf water from the Adélie Depression, East Antarctica. *Journal of Geophysical Research*, *113*, C04039. https://doi.org/10.1029/2007JC004346

Williams, G. D., Meijers, A. J. S., Poole, A., Mathiot, P., Tamura, T., & Klocker, A. (2011). Late winter oceanography off the Sabrina and BANZARE coast (117–128 E), East Antarctica. *Deep-Sea Research, Part II*, *58*(9-10), 1194–1210. https://doi.org/10.1016/j.dsr2.2010.10.035

Wong, A., Keeley, R., Thierry, C., & the Argo Data Management Team (2018). Argo Quality Control Manual For CTD and Trajectory Data. https://doi.org/10.13155/33951

Wong, A. P. S., & Riser, S. C. (2011). Profiling float observations of the upper ocean under sea ice off the Wilkes Land coast of Antarctica. *Journal of Physical Oceanography*, *41*(6), 1102–1115. https://doi.org/10.1175/2011JPO4516.1

Zhang, X., Thompson, A. F., Flexas, M. M., Roquet, F., & Bornemann, H. (2016). Circulation and meltwater distribution in the Bellingshausen Sea: From shelf break to coast. *Geophysical Research Letters*, *43*, 6402–6409. https://doi.org/10.1002/2016GL068998